Three-Phase Grid Connected Shunt Active Power Filter Based on Adaptive Q-LMF Control Technique

Kanchan Bala Rai, Narendra Kumar, *Senior Member, IEEE*, and Alka Singh, *Senior Member, IEEE*

***Abstract*—This article discusses the effectiveness of quantum calculus-based least mean fourth (q-LMF) based control for a 3∅ grid-connected photovoltaic (PV) shunt active power filter (SAPF). A PV array is utilized in the proposed system. Using the q-LMF-based controlling approach, the fundamental active load component is derived through the load current. The conventional LMF-based control scheme has been modified with the addition of the parameter "q". The variation of "q" influences the working performance of the designed controller. A modified complex coefficient filter is used to extract the filtered point of common coupling (PCC) voltage under a weak and distorted grid. In the current control mode, the SAPF feeds the appropriate compensatory current at the PCC to minimize current harmonics from the supply structure. The article also demonstrates real-time training of the algorithm for different q-LMF factors. The proposed system is initially modeled in MATLAB/Simulink, and the simulation results are validated using experimental findings. A hardware SAPF prototype is developed utilizing current/voltage sensors and MicroLabBox. Furthermore, a comparison of the least mean square, LMF, and the proposed q-LMF-based load compensation control method has been tested under steady-state conditions, load unbalancing, and weak grid. The three control schemes are analyzed in terms of convergence time, oscillations, source current total harmonic distortion (THD), and computational load. The proposed control scheme is found superior to others.**

***Index Terms*—Adaptive neural network, power quality, q calculus, quantum calculus-based least mean fourth (q-LMF), shunt active power filter (SAPF), Voltage Source Inverter (VSI).**

I. Introduction

INCREASED usage of electric vehicles, charging stations, storage systems, and distributed generators (DG) fueled by renewable energy has changed the traditional power system over the last ten years. The application of power electronic converters in connecting many DGs with adjacent loads is a novel concept for a "microgrid" [1], [2], [3], [4]. In [2], the response of the microgrid is discussed between grid-connected and islanded modes. The switching operation in both modes is discussed for the reactive power control. In [3], the microgrid using master/slave control consists of a storage system, photovoltaic (PV) system, and loads, and can be operated in either grid-connected mode or islanded mode. In [4], microgrid operation can be categorized into grid-connected and islanding modes. Power quality issues in the distribution system are caused by the increased penetration of nonlinear loads such as diodes and thyristor-based circuits [5]. The designing of shunt active power filter (SAPF) for pulsating load demands is discussed [6]. Power quality (PQ) issues, reactive power burden, poor power factor (PF), voltage harmonics, current harmonics, and increased heating have decreased the system's overall efficiency. A novel technology called a shunt active power filter is used in the electrical grid to address reactive power, harmonic distortions, and other problems related to power quality. It functions by introducing compensating currents into the system, which effectively reduces disturbances and assures a reliable power source.

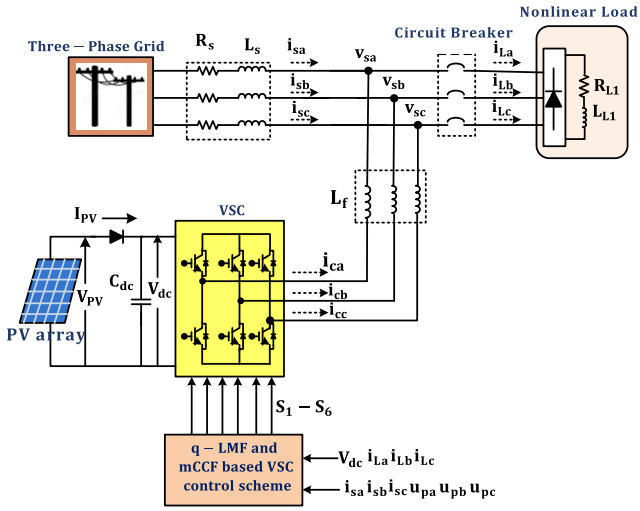

Fig. 1. System configuration of 3∅ grid-connected PV SAPF.

SAPF offers qualities such as customized filtering, flexibility to perform under system disturbances, and fast dynamic response and becomes an ideal solution for minimizing current-related power quality difficulties [7]. It is also noteworthy that active power filters operate more efficiently than under light loads [8]. Fig. 1 shows a PV-connected SAPF model that includes a **3** ∅ power supply, customer loads, and a voltage source inverter (VSI) in shunt with the source. SAPF is suitably controlled to inject equal amplitude harmonics into the current with a 180° phase shift so that the grid current is devoid of harmonics.

Power quality concerns may be classified as current- or voltage-related difficulties, and they can cause malfunction of end-user equipment. The PQ issues associated with current are current harmonics, reactive power utilization, and inadequate power factor. The PQ aspects related to voltage include voltage sags, voltage swells, notches, voltage harmonics, flickers, and so on. The ratio of the root mean square of the harmonic content,

Manuscript received 21 June 2023; revised 6 December 2023, 24 January 2024, and 26 March 2024; accepted 4 May 2024. Date of publication 8 May 2024; date of current version 20 June 2024. Recommended for publication by Associate Editor J. He. *(Corresponding author: Kanchan Bala Rai.)*

The authors are with the Department of Electrical Engineering, Delhi Technological University, Delhi 110042, India (e-mail: kanchan_2k19 phdee503@dtu.ac.in; narendrakumar@dtu.ac.in; alkasingh@dce.in).

Color versions of one or more figures in this article are available at https://doi.org/10.1109/TPEL.2024.3398369.

Digital Object Identifier 10.1109/TPEL.2024.3398369

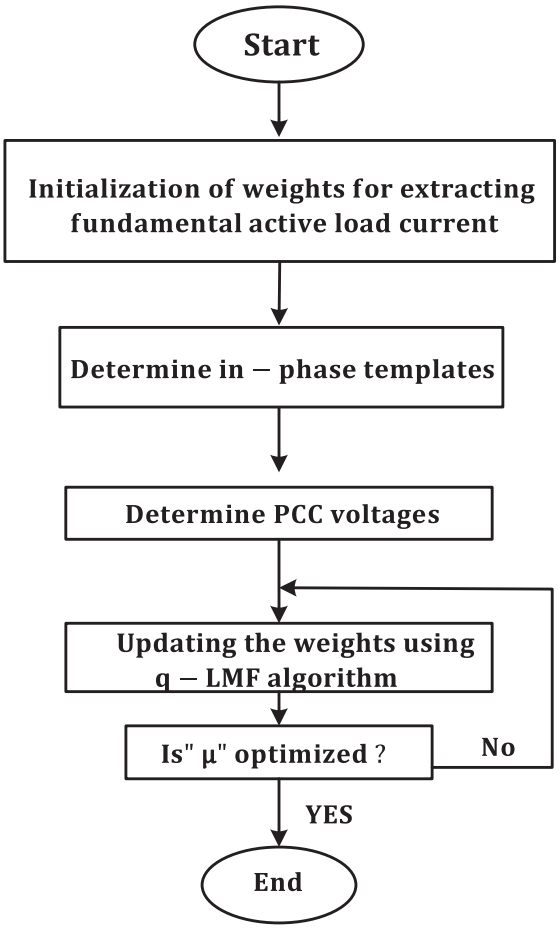

Fig. 2. Process diagram for utilizing the q-LMF controlling scheme to determine the ideal weight.

considering harmonic components up to the 50th order and specifically excluding interharmonics, is expressed as a percent of the fundamental. Harmonic components of order greater than 50 may be included when necessary. Several control strategies for SAPF have been discussed in the literature. The two most popular conventional control strategies are the instantaneous reactive power theory (IRPT) [9], and the synchronous reference frame (SRF) theory [10]. These two control schemes are used to calculate the fundamental load component for reference current generation for SAPF. The IRPT control scheme is discussed for power conditioning [11]. The SRF theory is also known as the dq theory because of its use of the phase-locked loop (PLL) and its foundation is based on the dq0 frame of reference. However, it is crucial to evaluate the SRF theory's efficacy in improving power quality aspects. The IRPT on the contrary, incorporates computations in a fixed reference frame without the usage of a PLL; as a result, it is widely used in the control of SAPF. The IRPT involves a much lower computation time as PLLs are not required. Some of the limitations of IRPT are sensitivity to harmonics, complexity implementation, and dynamic response issues. PQ enhancement of a single-phase grid-connected PV inverter is regulated using Bernoulli's polynomial-based artificial neural network controller [12]. In [13], the fundamental active load component extraction in shunt active power filtering is achieved via a Hermite polynomial-based controller. Another important current control technique is based on a second-order generalized integrator for harmonic extraction and a fuzzy-tuned PI controller for dc bus voltage [14]. Naqvi and Singh [15] proposed an enhanced filtering generalized integrator based filtering technique to filter the source voltage from harmonics content. This control scheme improves the PQ issues in grid-tied PV systems. Several maximum power point tracking (MPPT) algorithms have been developed for this purpose, to condition the control system to extract the maximum power point associated with the P-V and I-V characteristics of a PV module such as perturb and observation, hill climbing (HC), and Incremental Conductance. A modified decorrelation normalized least mean square (LMS) algorithm is used for load compensation to further generate the reference source current under various grid disturbance conditions [16].

The LMS control mechanism is commonly used as an adaptive controller in the DSTATCOM operation [17]. It is an adaptive filter. The properties of an unknown system in which this filter is used, as well as environmental changes, have propelled adaptive filter theory to the forefront of research. The presence of system perturbations leads to self-adjustment of the filter constants, ensuring that the system's filter and environment continue to function properly [18]. It is also well known that the normal LMS algorithm produces significantly more noise in the weights than the LMF approach when the time constant values for both techniques are identical. Hence, the approach is to achieve the right learning rule that produces a lower steady-state error and excellent tracking as compared to the conventional LMS-based control system [19].

A low signal-to-noise ratio restricts the LMS algorithm from reaching appropriate steady-state performance since it operates as a lower-order adaptive filter. Hence, to alleviate this difficulty and improve the system's steady-state performance, a fourth-order power expansion was used [20]. When evaluated against multiple inputs, the LMS algorithm is simpler to develop and provides consistent and reliable results. However, the LMS's rate of convergence is subpar [21]. A typical smaller step size is recommended to achieve the lowest possible error rate. An equilibrium is essential to achieve a faster convergence rate (CR), a lower step size, and better control performance. It is investigated that if CR is less than zero or approaches zero, the convergence rate is much better with better tracking capability as compared to CR equal to one. A conflict between these two algorithmic objectives can be overcome by selecting an appropriate convergence coefficient [22]. Numerous academics have been drawn to changes in its control parameters. The most popular and widely used LMS algorithms for improving power quality include normalized LMS, leaky LMS, variable step size LMS, kernel LMS, and Least mean mixed norm (LMMN) [23].

These algorithms allow self-governing tracking, reduced real-time processing, robustness to changes in system parameters, and good response even under dynamic load conditions. In terms of mean square error, adaptive algorithms with high-order errors, such as LMF perform better than conventional LMS algorithms (MSE). In [24], a new family of q-least mean fourth (q-LMF) based control-based stochastic gradient algorithms for channel identification is proposed. The q-LMF method, on the q-calculus, also referred to as Jackson's derivative, expands the LMF technique even further. The q-LMS algorithm has also been applied to the development of whitening filters and system identification [25]. The suggested algorithm in this study provides a new way to error correlation energy to give a quick convergence rate, enhanced stability and reduced steady-state error. In [26], comparison to traditional LMF, the suggested method provides higher flexibility even under larger step sizes. The q-steepest

descent approach is used to improve the stochastic gradient descent technique, which is frequently implemented in LMF or LMS-based control schemes. The standard LMF algorithm can achieve higher convergence than the LMS technique. It has been utilized successfully in various fields, including number theory, adaptive filtering, operational theory, mechanics, and relativity theory [27]. The proposed technique modifies the LMF approach to reduce the fourth power of the instantaneous error estimate.

The weighted sum of the inputs is sent to the summation unit. If the estimated output differs from the desired output, the weights are adjusted based on the obtained errors. Based on the error, the q-LMF learning algorithm adjusts the weight. To minimize errors and update weights, a q-LMF adaptive learning filter is utilized. The step size influences how fast the q-LMF converges. The proposed q-LMF is used for extracting the fundamental load component of each phase of the system, which is added with an active loss component and further used to generate reference source current for each phase.

A. Research Gap

1) Nonlinear loads cause power quality (PQ) issues; however, it is important to adhere to PQ regulations.
2) Conventional adaptive filtering algorithms show poor steady-state and dynamic responses under load unbalancing.

B. Technical Motivation

1) Evaluate the viability of the proposed control technique in a 3∅ grid-connected PV SAPF under load unbalancing while maintaining the PQ.
2) Application of q-LMF adaptive filter for PQ improvement.
3) Adding a control parameter q to typical LMF and LMS may improve performance while retaining system stability.
4) A comparative study among LMS, LMF, and *q*-LMF-based algorithms has been performed.

II. System Configuration

The proposed layout includes mostly a 3∅ VSI, a dc link capacitor (C_{dc}), interfacing inductor (L_f), source impedance (R_s, L_s), and a nonlinear load (R_{L1}, L_{L1}). There are six insulated gate bipolar transistors (IGBTs) in the VSI. For low to medium-power applications, IGBTs are a great solution. A PV array of 8.3 kW ratings is linked with the VSI. The PV power is fed to the grid through 3∅ VSI. The VSI is linked to the PCC employing an interface inductor (L_f). The nonlinear load is made up of a diode bridge rectifier with an R-L load. The switching signals for VSI switches are extracted through a proper control scheme designed based on the q-LMF algorithm. The total load current is estimated by summing the fundamental load current as well as the dc-link loss component. The resulting output is then multiplied with the unit template of each phase to obtain the reference source current. The six switching signals are generated after comparing the three reference source currents with the actual source currents. The switching pulses required by IGBTs are generated by the q-LMF control technique, as explained in Section III.

III. Control Algorithm

The proposed article utilizes a q-LMF-based control scheme to find the fundamental component of nonlinear load current. The control scheme is developed using a mathematical model with a suitable step size. By employing an extra control parameter q, the proposed q calculus-based LMF can be used to improve the performance of the traditional LMF while maintaining the algorithm's stability [24]. Furthermore, the proposed control technique generates adaptive weight values as shown in Fig. 2. If $q = 1$, the proposed q-LMF algorithm acts as a conventional LMF. However, the change in the q parameter can alter the behavior of the algorithm entirely.

A. Introduction to Q-Calculus

Quantum calculus is often known as limitless calculus. The differential of a function is expressed as

$$d_q\left(f\left(x\right)\right) = f\left(qx\right) - f\left(x\right). \tag{1}$$

The derivative of (1) is given as

$$D_q\left(f\left(x\right)\right) = \frac{d_q\left(f\left(x\right)\right)}{d_q\left(x\right)} = \frac{f\left(qx\right) - f\left(x\right)}{\left(q-1\right)x}. \tag{2}$$

If q tends to 1, the above expression is suited to the classical derivative. The q-gradient of function f(x) for "m" number of variables is expressed as [23]

$$\nabla_{q,w} f\left(x\right) \triangleq \left[D_{q1,x1} f\left(x\right), D_{q2,x2} f\left(x\right), \ldots\ldots\ldots D_{qn,xm} f\left(x\right)\right]^T$$

where $q = \left[q_1, q_2, q_{3\ldots\ldots\ldots\ldots}, q_m\right]^T$.

B. Proposed Adaptive q-LMF Algorithm

The conventional LMF algorithm is expressed as

$$w\left(n+1\right) = w\left(n\right) - \frac{\mu}{4}\nabla_w J\left(w\right) \tag{3}$$

where "μ" is the step size or learning rate, J(w) is the cost function for the proposed q-LMF algorithm, and it is expressed as $J(w) = e^4(n)$. Here, e(n) is defined as the calculated error between actual output (d) and calculated output $(w^T(n)x(n))$ at the *n*th instant. Also, x(n) is denoted as the input signal, which is expressed as $x(n) = \left[x_1, x_{2,\ldots\ldots\ldots\ldots\ldots}, x_M\right]^T$

$$e\left(n\right) = d\left(n\right) - w^T\left(n\right)x\left(n\right) \tag{4}$$

and "w" is the weights vector, and "M" is the length of the filter. The proposed q-LMF algorithm is obtained by replacing the conventional gradient with the q-gradient [21]

$$w\left(n+1\right) = w\left(n\right) - \frac{\mu}{4}\nabla_{q,w} J\left(w\right) \tag{5}$$

$$\nabla_{q,w} J\left(w\right) = -4E\left(q_K^3 + q_K^2 + q_K^2 + 1\right) x_K\left(n\right) e^3\left(n\right), \quad \text{for } K = 1, 2, 3, \ldots..M \tag{6}$$

$$\nabla_{q,w} J\left(w\right) = -4E\left[Gx\left(n\right) e^3\left(n\right)\right] \tag{7}$$

where q_k is the quiescent value at *k*th instant of time, G is a diagonal matrix

$$\text{diag}\left(G\right) = \left[\left(\frac{q_1^3 + q_1^2 + q_1 + 1}{4}\right), \left(\frac{q_2^3 + q_2^2 + q_2 + 1}{4}\right), \ldots\ldots\ldots\ldots, \left(\frac{q_M^3 + q_M^2 + q_M + 1}{4}\right)\right]^T. \tag{8}$$

Because of system ergodicity $\nabla_{q,w} J(w)$ can be expressed as $\nabla_{q,w} J(w) \approx -4Gx(n)e^3(n)$. Equation (5) will be expressed as

$$w\left(n+1\right) = w\left(n\right) + \mu Gx\left(n\right) e^3\left(n\right). \tag{9}$$

The input variable x(n) is given by

$$x\left(n\right) = \left[u_{pa} u_{pb} u_{pc}\right]^T \tag{10}$$

$$e(n) = \begin{bmatrix} i_{La}(n) - u_{pa}(n) w_{pa}(n) \\ i_{Lb}(n) - u_{pb}(n) w_{pb}(n) \\ i_{Lc}(n) - u_{pc}(n) w_{pc}(n) \end{bmatrix} \quad (11)$$

$$w(n+1) = \left[w_{pa}(n+1)\, w_{pb(n+1)} w_{pc}(n+1) \right]^T \quad (12)$$

$$w(n) = \left[w_{pa}(n)\, w_{pb}(n)\, w_{pc}(n) \right]^T \quad (13)$$

where in-phase unit templates are represented by u_{pa}, u_{pb}, u_{pc}. e(n) is defined as the difference between the real load current $i_{Lk}(n)$ and calculated load current $i'_{Lk}(n) = [u_{pk}(n) \times w_{pk}(n)]$ (k = a, b, c), $w_{pk}(n)$ is the active weight component.

The weight of the fundamental active component of the load current of phase "a" is expressed as

$$w_{pa}(n+1) = w_{pa}(n) + \mu G u_{pa}\left(\left(e_{pa}(n) \right)^3 \right). \quad (14)$$

Similarly, for phases "b" and "c"

$$w_{pb}(n+1) = w_{pb}(n) + \mu G u_{pb}\left(\left(e_{pb}(n) \right)^3 \right) \quad (15)$$

$$w_{pc}(n+1) = w_{pc}(n) + \mu G u_{pc}\left(\left(e_{pc}(n) \right)^3 \right). \quad (16)$$

For LMF-based operations, $q_1, q_2, q_3 = 1$

$$G = [1\ 1\ 1]^T.$$

While for q-LMF, the value of q can be chosen according to the requirement q = 2, 3, 4 … …..

For $q_1, q_2, q_3 = 2$

$G = [3.5\ 3.5\ 3.5]^T$ using (8).

Hence, the G matrix is dependent on the choice of q.

C. Generation of Unit Templates and Reference Source Current

The active and reactive components of the load current have harmonics. The control strategy for producing switching signals using the q-LMF algorithm is shown in Fig. 3. The unit template must be in the same phase as the PCC voltage. The mCCF is used to obtain a sinusoidal unit template under abnormal grid conditions. The Transfer function of mCCF is given by

$$T(s) = \omega_c \frac{(s + \omega_c + j\omega_0)}{(s + \omega_c)^2 + \omega_0^2} \quad (17)$$

where ω_c, ω_0 is the bandwidth of CCF and favourable angular frequency of CCF, respectively. The values selected for where ω_c, ω_0 are 94.2 and 314 rad/se. This filtered fundamental source voltages $(v'_{sa}, v'_{sb}, v'_{sc})$ are used to generate the unit templates (u_{pa}, u_{pb}, u_{pc})

$$u_{pa} = \frac{v'_{sa}}{V_t}, u_{pb} = \frac{v'_{sb}}{V_t}, u_{pc} = \frac{v'_{sc}}{V_t} \quad (18)$$

$$V_t = \sqrt{{v'_{sa}}^2 + {v'_{sb}}^2 + {v'_{sc}}^2} \quad (19)$$

where V_t denotes the PCC voltage amplitude. Using (18), the proposed work implements a PLL-less control system. The active loss component $I_P(n)$ is calculated by subtracting the reference dc-link voltage (V^*_{dc}) and actual dc-link voltage (V_{dc}). The active loss component is expressed as

$$I_P(n+1) = I_P(n) + K_I V_{dce}(n+1) + K_p(V_{dce}(n+1) - V_{dce}(n) \quad (20)$$

$$V_{dce}(n) = V^*_{dc}(n) - V_{dc}(n) \quad (21)$$

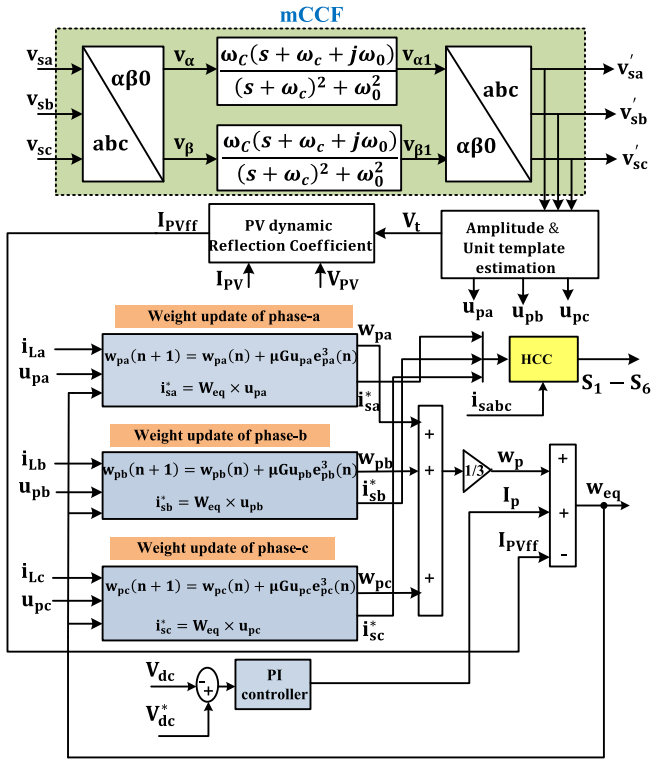

Fig. 3. Control approach based on adaptive q-LMF for generating switching signals for a three-phase grid-connected PV system.

where K_I, K_p are the integral and proportional gains utilized to tune the PI voltage controller on the dc-link. The addition of the average fundamental active weight component (w_p), the dc loss component (I_P) are added and the PV's feedforward current (I_{PVff}) is subtracted from the total gives the total active component $(w_{eq})$of 3∅ source current determined as

$$w_{eq} = w_p + I_p - I_{PVff} \quad (22)$$

$$w_p = (w_{pa} + w_{pb} + w_{pc})/3. \quad (23)$$

The PV feedforward current is utilized for compensating the performance under current and voltage disturbance and it is expressed as

$$I_{PVff} = \frac{2P_{PV}}{3V_t}. \quad (24)$$

The active reference source current is defined as

$$i^*_{sa} = w_{eq} * u_{pa}; i^*_{sb} = w_{eq} * u_{pb}; i^*_{sc} = w_{eq} * u_{pc}. \quad (25)$$

The reference source current (i^*_{sabc}) is obtained by using

$$i^*_{sabc} = [i^*_{sa}\ i^*_{sb}\ i^*_{sc}] \quad (26)$$

where $i^*_{sa}, i^*_{sb}, i^*_{sc}$ are the 3∅ reference source current.

IV. Results and Discussion

A hardware setup is developed in the laboratory using Hall effect current and voltage sensors LEM LA 25P and LEM LV 25P, respectively, as shown in Fig. 4. Sensor circuits measure each phase's source current, load current, dc link voltage, and source voltage. A digital signal processor for applied and control engineering (dSpace) controller (1202-DSPACE) is implemented to execute the control scheme. The nature of the sensor's output is analog, which must be changed into a digital signal through an

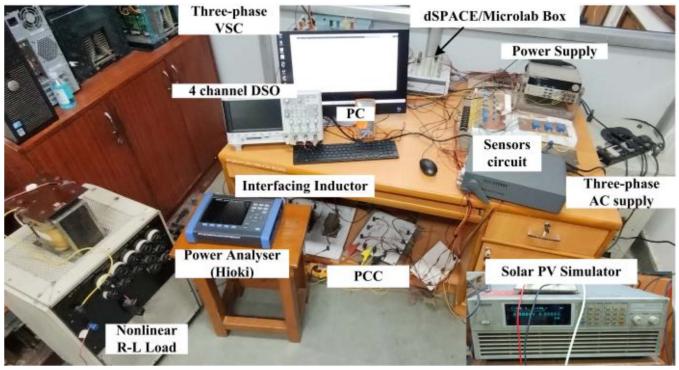

Fig. 4. Experimental setup of proposed 3∅ grid-connected PV-SAPF.

TABLE I
SYSTEM PARAMETERS

System Parameters	Simulation Value	Experimental Value
3∅ ac supply (line to line)	415 V (rms)	40 V (rms)
System frequency	50 Hz	50 Hz
Filter impedance $\mathbf{R_f, L_f}$	0.1 Ω, 4.3 mH	0.1 Ω, 4.3 mH
Source impedance $\mathbf{R_s, L_s}$	0.04 Ω, 1 mH	0.1 Ω, 3.5 mH
Reference dc-link voltage $V_{dc(ref)}$	800 V	80 V
Dc Capacitance ($\mathbf{C_{dc}}$)	1650μF	4700 μF
PI controller	K_P =0.4, K_I = 1.5	K_P =0.05, K_I = 0.005
learning rate (μ)	0.01	0.01
At $\mathbf{q = 2}$	G $= [3.75 \quad 3.75 \quad 3.75]^T$	G $= [3.75 \quad 3.75 \quad 3.75]^T$
Switching Frequency $\mathbf{f_{sw}}$	10 kHz	10 kHz
Three-phase uncontrolled diode rectifier with Load $\mathbf{R_{L1}, L_{L1}}$	40 Ω, 10 mH	20 Ω, 80 mH

A/D converter provided through MicroLabBox/dSpace. The PV characteristics is realized using a solar PV simulator (Chroma 62100H-600S). PV is integrated at the dc link of the three-phase VSC and synchronized with the grid. A power quality analyzer (Hioki-PQ 3100) is utilized for harmonic spectra analysis of current and voltage. For voltage and current measurements, voltage probes (HIOKI) and current probes (HIOKICT7136) are used. The dynamic response of the proposed system is captured using a digital signal oscilloscope (DSOX2014A). The sampling time of the proposed system is considered as 50 μs for running the experimental setup.

Also, the effectiveness of the proposed system is evaluated by simulating the proposed system in MATLAB Simulink. The simulation model consists of a 3∅ ac grid, 3∅ nonlinear loads, 3∅ VSI, and interfacing inductors coupled at the PCC along with the control scheme for the proposed system. The system parameters and their value are given in Table I. The effectiveness of a 3∅, grid coupled SAPF is modeled in MATLAB/Simulink under both steady-state and dynamic load conditions. The effectiveness of the proposed system is monitored using appropriate signals, such as source voltages (v_{sabc}), source currents (i_{sabc}), load currents (i_{Labc}), compensating current (i_{Cabc}), dc-link voltage (V_{dc}), active source power (P_S), source reactive power (Q_S), load active power demand (P_L), load reactive power demand (Q_L), and PV's active power (P_{PV}). The proposed current extraction method is used to evaluate SAPF behavior in both steady-state and dynamic modes. The proposed control strategy must be implemented on the VSI to improve the said power quality issues.

TABLE II
HARMONIC SPECTRA OF SOURCE VOLTAGE AND SOURCE CURRENT UNDER NONLINEAR LOAD DURING NORMAL AND WEAK GRID CONDITIONS

Conditions	Magnitude		Percentage THD	
	Source Voltage (v_{sa})	Source Current (i_{sa})	Source Voltage (v_{sa})	Source Current (i_{sa})
Normal Grid	338.8 V	12.6 A	0.63%	1.65%
Voltage Sag	271.1 V	18.97 A	0.85%	1.70%
Voltage Swell	406.6 V	4.497 A	0.54%	4.35%

The harmonic spectra of source voltage and source currents under normal and weak grids are given in Table II. The source voltage (v_{sa}) and source current (i_{sa}), have a total harmonic distortion (THD) of 0.63% and 1.65%, respectively, under a normal grid while the THD of i_{sa} under voltage sag and swell are 1.7% and 4.35%, respectively, as given in Table II. The source voltage and source current are in phase with one another, maintaining the PF at unity. The SAPF's functioning has provided compensation for the load's reactive power demand (Q_L) and reduces the harmonics in the source currents. The VSI compensates by supplying the necessary current computed using the proposed algorithm.

Even when the load is unbalanced, the supply current tries to be sinusoidal. It is also observed that the active component weight varies owing to load variations, and the error signal fluctuates close to zero before recovering to its starting value.

A. Voltage Swell, Voltage Sag, Distorted Grid, and Load Unbalancing

The performance of the proposed system under voltage sag is shown in Fig. 5. The three-phase source voltage (v_s) is deviated from its nominal value by approximately 20% of the actual voltage. Due to the constant source power supply, the source current (i_{sabc}) is increased as noticed in Fig. 5. The voltage at PCC is decreased at voltage sag due to which voltage across load decreases and, hence, load current decreases. The dc link voltage is maintained at its reference value due to its control scheme. The power from the PV array fulfills the load demand and the remaining power is supplied to the grid.

Fig. 5 illustrates the suggested system's operation under voltage sag, swell, and distorted grid. There is a 20% deviation between the nominal and actual values of the three-phase source voltage (v_{sabc}). As seen in Fig. 5, the source current (i_{sabc}) decreases because of the continuous source power delivery under voltage swell conditions. When there is a voltage swell, the voltage at the PCC increases, which increases the voltage across the load and, consequently, the load current. Its control mechanism keeps the dc link voltage at its reference level. The source current maintains to be sinusoidal under load unbalancing conditions. The THD of the source voltage (v_{sa}) and source current (i_{sa}) are 0.85%, 1.70%, respectively, under voltage sag. The THD of the source voltage (v_{sa}) and source current (i_{sa}) are 0.54%, 4.35%, respectively, under voltage swell as shown in Fig. 6, which are below the IEEE-519 standards' allowable limit.

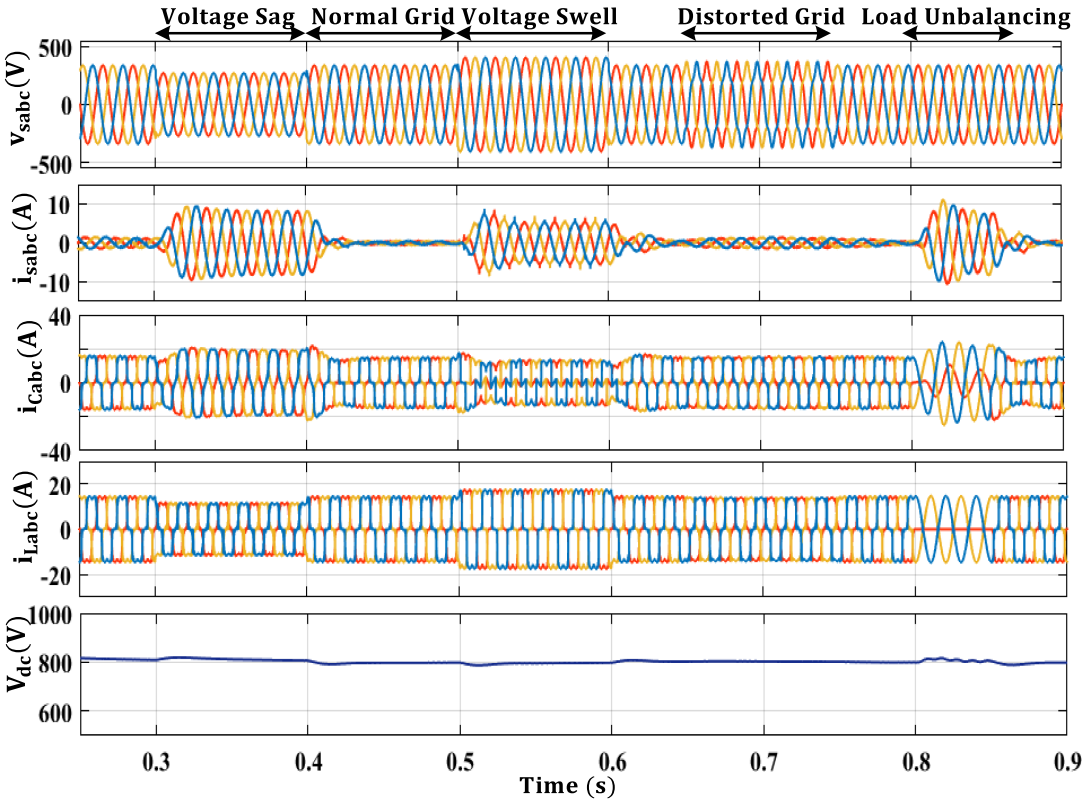

Fig. 5. Waveforms under the normal grid, voltage sag, voltage swell, voltage harmonics at source voltage and load unbalancing.

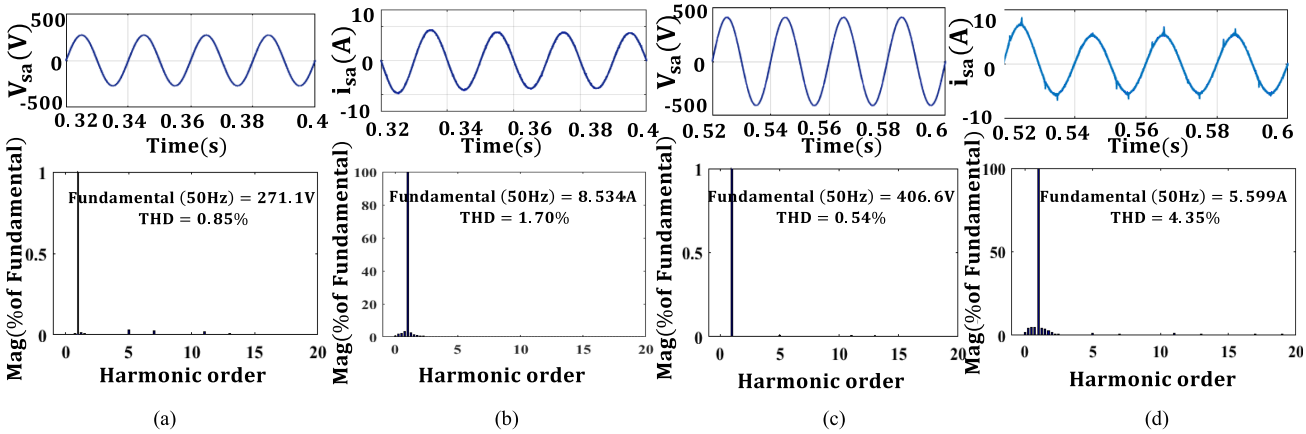

Fig. 6. FFT analysis of source voltage and source current under (a) and (b) v_{sa} and i_{sa} under voltage sag (c) and (d) v_{sa} and i_{sa} under voltage swell.

The source current under a distorted grid at t = 0.65 s, the source current remains sinusoidal with the effect of the control scheme. The THD of the source current (i_{sa}) under distorted source voltage is 2.40%, and THD of source voltage (v_{sa}) is 10.04%, as shown in Fig. 7.

The power analysis under the weak grid and normal grid is shown in Fig. 8. The solar PV is connected to VSC at 1000 W/m^2 irradiance. The waveforms of signals PV voltage (V_{PV}), PV current (I_{PV}), active source power (P_S), source reactive power (Q_S), load active power demand (P_L), load reactive power demand (Q_L), VSC's reactive power (Q_L), and solar PV array (P_{PV}). The active (P_L) and reactive load power (Q_L) demand are fulfilled by PV array and VSI, respectively. While the extra PV's power is fed to the grid.

B. Comparison of the Proposed Q-LMF-Based Control With Conventional Adaptive Control Algorithms

Fig. 9(a) shows the fundamental active weight component waveform under steady-state conditions. This is found that the fundamental weight signal converges fast with the q-LMF-based algorithm. Fig. 9(b) shows the response of the average weight of the fundamental component of load current (w_p) to load unbalancing in phase "a" for the proposed q-LMF-based control algorithm. Studies demonstrate that by adding a second regulating term, "q" to the traditional LMF technique, the developed q-LMF algorithm enhances its performance. The comparative analysis considers step size $\mu = 0.01$ for LMS, LMF, and q-LMF with different values of q = 1, 2, 3. The effectiveness of the

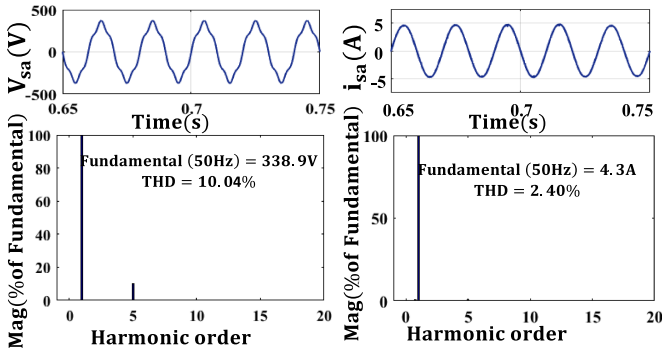

Fig. 7. FFT analysis under Distorted grid condition (a) source voltage and (b) source current.

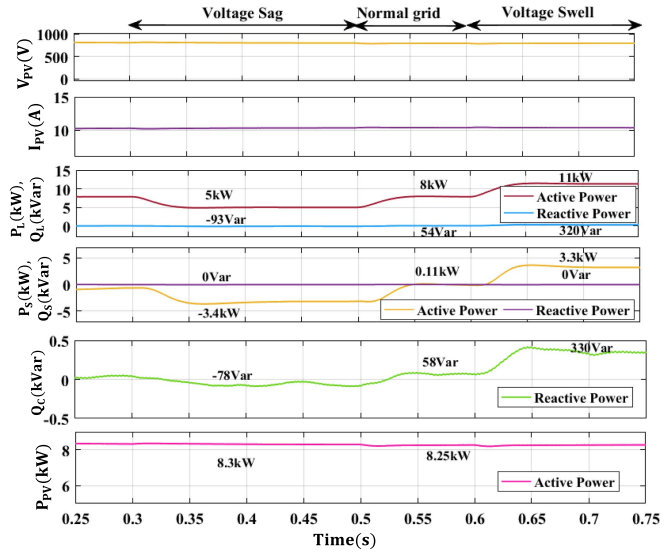

Fig. 8. Power analysis under weak and normal grid conditions.

algorithms is investigated in terms of steady-state error and convergence rate and Fig. 9(b) demonstrates that the q-LMF performs better than the traditional LMF and LMS. The proposed algorithm converges faster as compared to the conventional LMF and LMS. The average active component computed using the LMS technique takes the maximum time to reach the steady state with LMF and the proposed q-LMF techniques. Fig. 9(b) shows that the oscillations using the LMS technique are quite less but it causes the maximum error and tracking is erroneous, especially under unbalanced load conditions. Table IV illustrates the comparison among techniques such as LMS, LMF, LMMN, and q-LMF.

It is investigated from Table III, that proposed q-LMF has better performance than other conventional schemes. When $q = 2$, the signal converges at t = 0.54 s, and the q = 1(Conventional LMF) signal converges at t = 0.56 s. When q = 3, the fundamental active component of load current has fast convergence compared to q = 1 and 2 but with a small steady-state error. Hence, q = 2 has been selected as the optimized value. The investigations reveal that the q-LMF algorithm response is highly dependent on the q parameter selected. From Fig. 9, it is clearly shown that by increasing the value of q, faster learning can be achieved but at the cost of significant error.

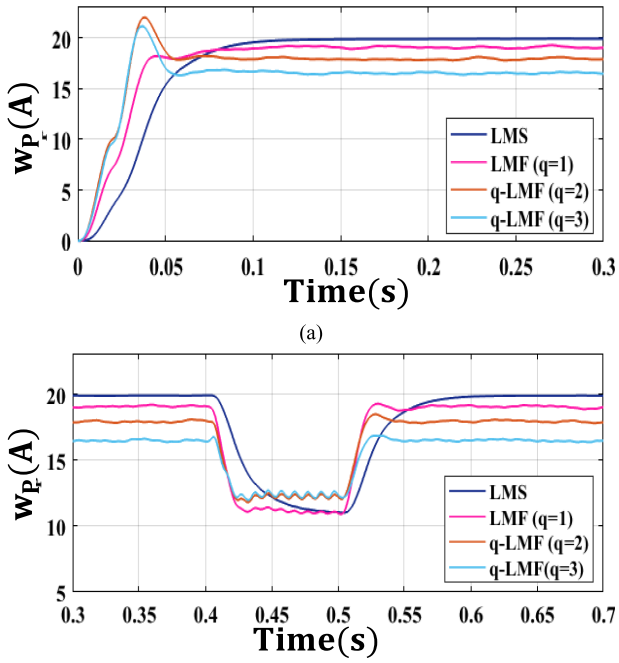

Fig. 9. Response of fundamental weight signal (w_p) for conventional LMF, LMS, and proposed q-LMF (at q = 2, q = 3) at (a) steady state and (b) dynamic load condition.

TABLE III
COMPARATIVE STUDY OF PROPOSED CONTROL (Q-LMF) ALGORITHM WITH CONVENTIONAL CONTROL SCHEME

Parameter	Conventional control Algorithm			Proposed Control
	LMS	LMF	LMMN	*q*-LMF
Type	Adaptive	Adaptive	Adaptive	Adaptive
Complexity	Low	Low	Moderate	Low
Order of optimization	Second	Fourth	Mixed (Second and Fourth)	Fourth
Oscillation a. Steady-state b. Transient state	 No No	 Moderate Moderate	 Moderate Moderate	 Lesser Moderate
Sampling Time (Ts)	60 µs	50 µs	55 µs	50 µs
Convergence Time	more	moderate	moderate	less

TABLE IV
CONVERGENCE ANALYSIS AMONG LMS, LMF, AND Q-LMF CONTROL SCHEME

Technique	Steady-state condition		Dynamic condition	
	Error	Convergence Time	Error	Convergence Time
LMS	0.2 A	100 ms	0.27 A	76 ms
LMF (q = 1)	0.5 A	88 ms	0.27 A	58 ms
q-LMF (q = 2)	1.2 A	64 ms	0.62 A	42 ms
q-LMF(q = 3)	4.1 A	52 ms	3.02 A	29 ms

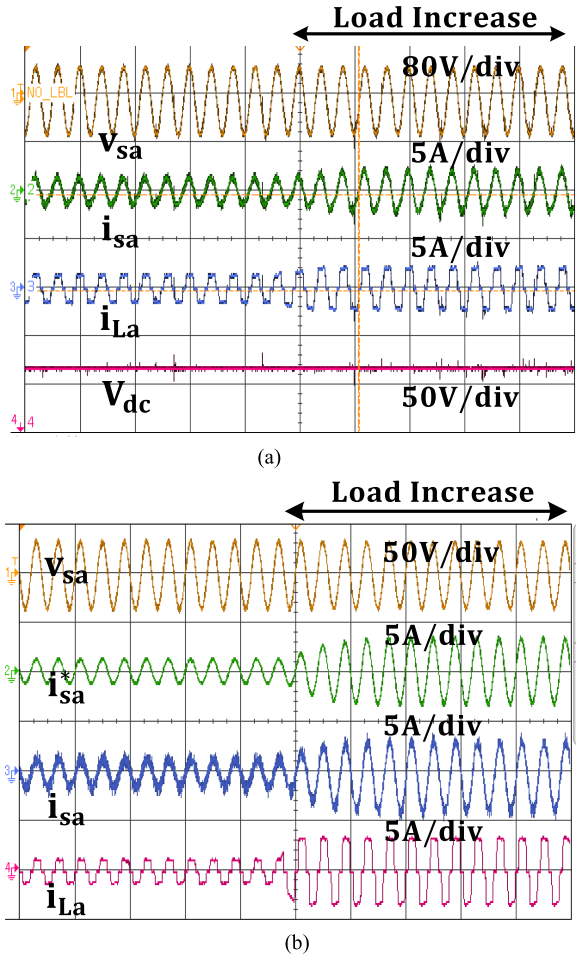

Fig. 10. (a) Dynamic response of the proposed system having waveforms of signals v_{sa}, i_{sa}, i_{La}, and V_{dc}. (b) Source voltage (v_{sa}), reference source current (i^*_{sa}), actual source current (i_{sa}), and load current (i_{La}) of phase-a under load unbalancing.

C. Experimental Results

Dynamic response of the proposed system with q-LMF control scheme is shown in Fig. 10. Fig. 10(a) shows the dynamic response of the system under load increase. The waveform of signals of phase "a" source voltage (v_{sa}), source current (i_{sa}), load current (i_{La}), and dc link voltage (V_{dc}) are shown in Fig. 10(a). The source current decreases as the decrease in load to maintain the supply power constant. At the same time, the dc link voltage regulates its reference value due to the effectiveness of the PI controller. The dc link voltage slightly decreases with an increase in load for almost a cycle; after that, it will regulate to its reference 80 V, as shown in Fig. 10(a). The reference source current (i^*_{sa}) is sinusoidal and follows the sensed source current due to the proposed q-LMF control and HCC, as shown in Fig. 10(b). The proposed system is also tested under weak grid conditions, i.e., voltage sag, swell and distorted grid. A 20% of voltage sag and swell are observed on the PCC voltage, as shown in Fig. 11(a) and (b). It is notified from the Fig. 11(a), the phase "a" source voltage (v_{sa}) is decreased due to voltage sag at PCC. The source current (i_{sa})increase to maintain the supply power (P_L) constant. Because the load power is proportional to the square of source voltage, the load power, as well as load current, decreases and vice-versa in case of voltage swell. The distorted voltage in the source voltage is shown in Fig. 11(b). It is seen

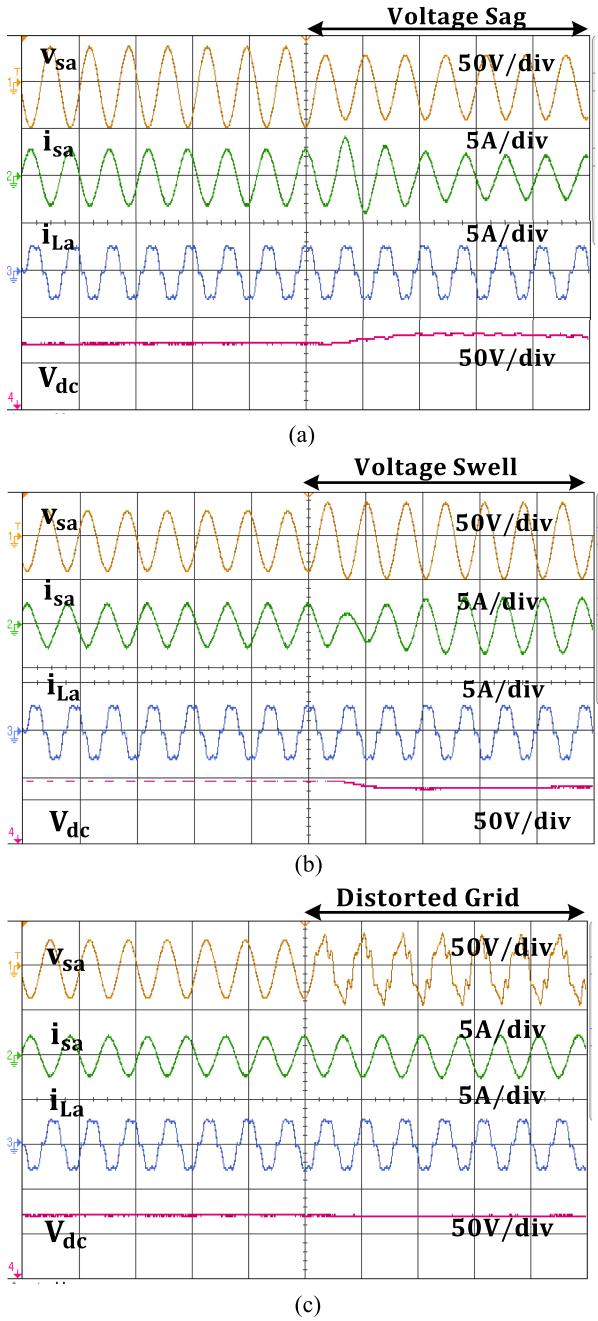

Fig. 11. Performance analysis of proposed control scheme under (a) voltage sag, (b) voltage swell, and (c) distorted voltage.

that the source current is sinusoidal due to the proposed control scheme. The proposed system behaves satisfactorily under weak and distorted grid condition due to mCCF at the input of PCC voltage, which filter out the unwanted harmonic component and extract the fundamental component of source voltage. The dc link voltage is maintained to its reference value.

The intermediate signals of the proposed control scheme based on q-LMF are shown in Fig. 12(a). The effectiveness of q calculus-based LMF on fundamental active load components under load unbalancing is shown in Fig. 12(b).

The conventional LMF takes more time to converge under load unbalancing and reach a steady state. The conventional LMF takes around 4.5 cycles to reach the steady state position, while with q-LMF with q = 2, G = 3.5,

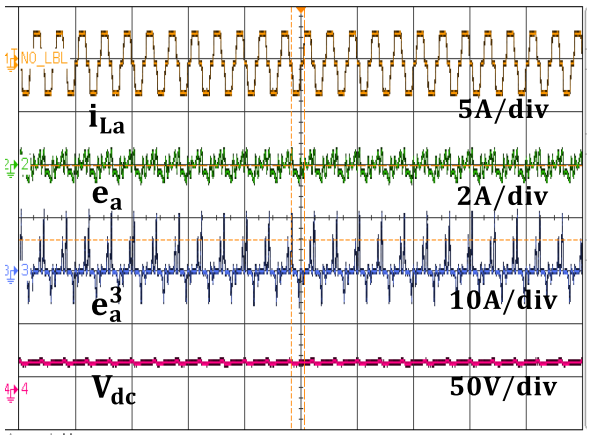

(a)

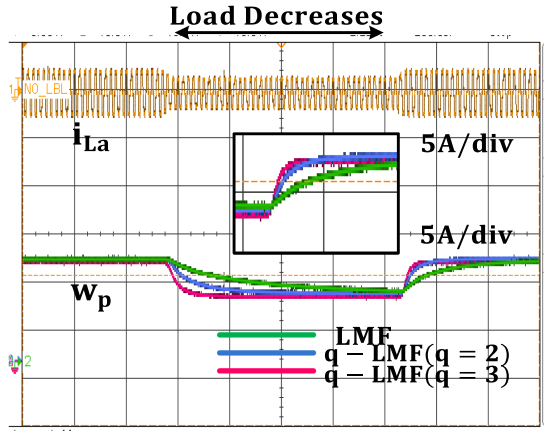

(b)

Fig. 12. Intermediate signals of the proposed q-LMF-based control scheme with the waveforms of (a) i_{La}, e_a, e_a^3, and V_{dc} and (b) fundamental weight w_p under load change.

the fundamental active load component takes 1 to 1.5 cycles to converge. When q = 3, the fundamental active components converge the fastest but a small steady-state error is also obtained. When $q = 2$, both convergence rate and steady-state performance are optimized. Thus, it is established from Fig. 12(b) that increasing the value of "q" results in fast convergence but also results in a large steady-state error. These results also match the findings of simulation studies. Fig. 13(a) and (b) shows the representations of source voltage and source current with current THD levels. The THD of the source current is achieved to be 2.99% with SAPF compensation and follows the IEEE 519 standards, while the THD of the source voltage is only 1.15%. Fig. 13(c) and (d) shows the source voltage waveform and load current with THD, respectively. The THD of load current is 21.63%.

V. Conclusion

The proposed control scheme is based on the q-LMF adaptive filter technique. The proposed control scheme is developed and implemented on developed prototype for grid connected PV system. With a single-stage, three-phase grid-integrated PV system that is exposed to nonlinear loading at voltage swell, voltage sag, load imbalance, and distorted voltages at PCC, the q-LMF has

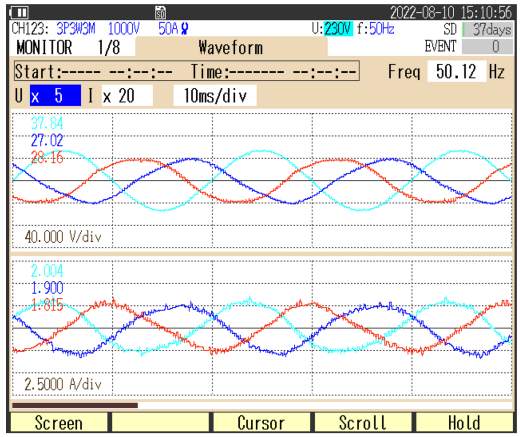

(a)

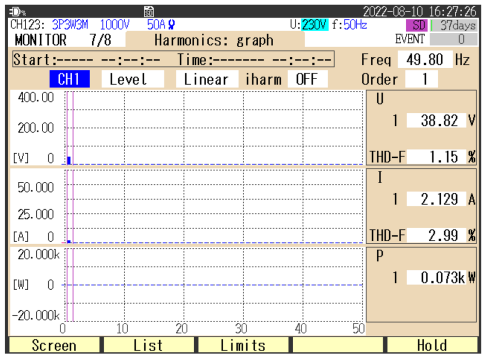

(b)

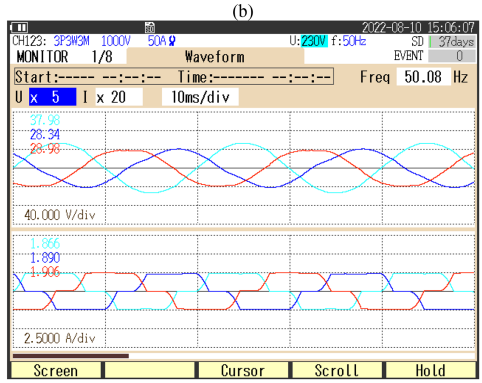

(c)

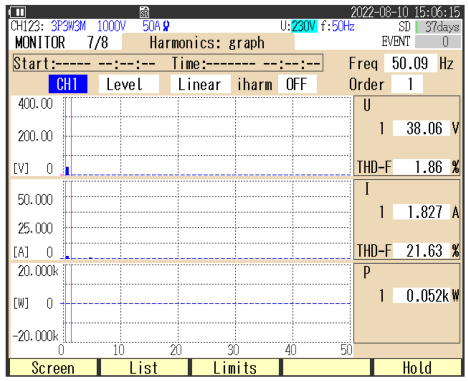

(d)

Fig. 13. Power analyzer results of (a) waveforms of the source voltage and current, (b) THD of source current, (c) waveforms of source voltage and load current, and (d) THD of load current.

increased power control capabilities and improved power quality. The proposed control scheme includes an extra parameter q and offers more control over the dynamic performance and rate of convergence. The conventional LMF is also compared with the *q*-LMF for power quality improvement. The simulation and experimental results have shown that the THD of the source current is well within IEEE-519: 2014 limits and a proper power balance has been achieved between the source, load, and inverter. The response of the proposed controller has proven to be effective and reliable compared with existing conventional techniques. The effectiveness of the proposed *q*-LMF-based control technique (with q = 2) resulted in optimized performance with a fast convergence rate and the least steady-state error in the estimation of the fundamental active weight component of load current. The MSE obtained with *q*-LMF showed a lower value than the conventional LMF control. The developed PQ controller maintains the power factor of the source current to unity as well as makes the source current sinusoidal. During load unbalancing conditions, the dc-link voltage is well regulated within 10%, and reactive power compensation is accomplished by efficiently using the proposed q-LMF control method. Significant features of the proposed *q*-LMF technique for load compensation and weak grid are presented.

1) The *q*-LMF technique is similar to a single-layer training technique for online weight updating to derive the fundamental component of the load current from the distorted load current.
2) It has a PLL-less structure.
3) It provides appropriate switching signals irrespective of load uncertainties and weak grid.
4) It offers a higher convergence rate, lower steady-state error, and better dynamic performance as compared to conventional techniques.
5) The proposed technique is effective in improving power quality issues.

ACKNOWLEDGMENT

The authors would like to thank to the DST for project SR/FST/ET-I/2022/1026.

REFERENCES

[1] A. C. Moreira, H. K. M. Paredes, W. A. de Souza, F. P. Marafao, and L. C. P. da Silva, "Intelligent expert system for power quality improvement under distorted and unbalanced conditions in three-phase AC microgrids," *IEEE Trans. Smart Grid*, vol. 9, no. 6, pp. 6951–6960, Nov. 2018.

[2] K.-H. Tan, F.-J. Lin, C.-M. Shih, and C.-N. Kuo, "Intelligent control of microgrid with virtual inertia using recurrent probabilistic wavelet fuzzy neural network," *IEEE Trans. Power Electron.*, vol. 35, no. 7, pp. 7451–7464, Jul. 2020.

[3] K.-H. Tan and T.-Y. Tseng, "Seamless switching and grid reconnection of microgrid using Petri recurrent wavelet fuzzy neural network," *IEEE Trans. Power Electron.*, vol. 36, no. 10, pp. 11847–11861, Oct. 2021.

[4] F.-J. Lin, K.-H. Tan, C.-F. Chang, M.-Y. Li, and T.-Y. Tseng, "Development of intelligent controlled microgrid for power sharing and load shedding," *IEEE Trans. Power Electron.*, vol. 37, no. 7, pp. 7928–7940, Jul. 2022.

[5] M. H. J. Bollen et al., "Power quality concerns in implementing smart distribution-grid applications," *IEEE Trans. Smart Grid*, vol. 8, no. 1, pp. 391–399, Jan. 2017, doi: 10.1109/TSG.2016.2596788.

[6] A. K. Panda and T. Penthia, "Design and modeling of SMES based SAPF for pulsed power load demands," *Int. J. Electr. Power Energy Syst.*, vol. 92, pp. 114–124, Nov. 2017, doi: 10.1016/j.ijepes.2017.04.011.

[7] J. Monroy-Morales, D. Campos-Gaona, M. Hernández-Ángeles, R. Peña-Alzola, and J. Guardado-Zavala, "An active power filter based on a three-level inverter and 3D-SVPWM for selective harmonic and reactive compensation," *Energies*, vol. 10, no. 3, Mar. 2017, Art. no. 297, doi: 10.3390/en10030297.

[8] M. H. Rashid, N. Kumar, and A. Kulkarni, "Power Electronics Devices," *Circuits Appl.*, 2014, Art. no. 1027.

[9] S. K. Patel, S. R. Arya, R. Maurya, and B. C. Babu, "Control scheme for DSTATCOM based on frequency-adaptive disturbance observer," *IEEE J. Emerg. Sel. Topics Power Electron.*, vol. 6, no. 3, pp. 1345–1354, Sep. 2018.

[10] K. H. Tan, F. J. Lin, C. Y. Tsai, and Y. R. Chang, "A distribution static compensator using a CFNN-AMF controller for power quality improvement and DC-link voltage regulation," *Energies*, vol. 11, no. 8, pp. 1–17, 2018.

[11] H. Akagi, E. H. Watanabe, and M. Aredes, *Instantaneous Power Theory and Applications to Power Conditioning*, vol. 62. Hoboken, NJ, USA: Wiley, 2017.

[12] K. B. Rai, A. Singh, and N. Kumar, "Bernoulli polynomial-based control technique for PV-integrated grid system under distorted supply," *Int. J. Circuit Theory Appl.*, vol. 51, pp. 3204–3225, Mar. 2023, doi: 10.1002/cta.3578.

[13] K. B. Rai, N. Kumar, and A. Singh, "Design and analysis of Hermite function-based artificial neural network controller for performance enhancement of photovoltaic-integrated grid system," *Int. J. Circuit Theory Appl.*, vol. 51, no. 3, pp. 1440–1459, Mar. 2023, doi: 10.1002/cta.3486.

[14] N. Babu P., R. B. Peesapati, and G. Panda, "An adaptive current control technique in grid-tied PV system with active power filter for power quality improvement," in *Proc. TENCON 2019 - 2019 IEEE Region 10 Conf.*, 2019, pp. 187–191, doi: 10.1109/TENCON.2019.8929487.

[15] S. B. Q. Naqvi and B. Singh, "An enhanced filtering generalized integrator-based control for improved performance of a grid-tied PV system at adverse grid voltages," *IEEE Trans. Ind. Electron.*, vol. 70, no. 12, pp. 12376–12386, Dec. 2023, doi: 10.1109/TIE.2023.3239922.

[16] S. Pradhan, I. Hussain, B. Singh, and B. Ketan Panigrahi, "Performance improvement of grid-integrated Solar PV system using DNLMS control algorithm," *IEEE Trans. Ind. Appl.*, vol. 55, no. 1, pp. 78–91, Jan./Feb. 2019, doi: 10.1109/TIA.2018.2863652.

[17] M. Srinivas, I. Hussain, and B. Singh, "Combined LMS–LMF-based control algorithm of DSTATCOM for power quality enhancement in distribution system," *IEEE Trans. Ind. Electron.*, vol. 63, no. 7, pp. 4160–4168, Jul. 2016, doi: 10.1109/TIE.2016.2532278.

[18] E. Walach and B. Widrow, "The least mean fourth (LMF) adaptive algorithm and its family," *IEEE Trans. Inf. Theory*, vol. 30, no. 2, pp. 275–283, Mar. 1984, doi: 10.1109/TIT.1984.1056886.

[19] R. K. Agarwal, I. Hussain, and B. Singh, "LMF-based control algorithm for single stage three-phase grid integrated Solar PV system," *IEEE Trans. Sustain. Energy*, vol. 7, no. 4, pp. 1379–1387, Oct. 2016, doi: 10.1109/TSTE.2016.2553181.

[20] G. Gui, W. Peng, and F. Adachi, "Adaptive system identification using robust LMS/F algorithm," *Int. J. Commun. Syst.*, vol. 27, no. 11, pp. 2956–2963, Feb. 2013, doi: 10.1002/dac.2517.

[21] M. Badoni, A. Singh, and B. Singh, "Variable forgetting factor recursive least square control algorithm for DSTATCOM," *IEEE Trans. Power Deliv.*, vol. 30, no. 5, pp. 2353–2361, Oct. 2015, doi: 10.1109/TPWRD.2015.2422139.

[22] S. K. Patel, S. R. Arya, and R. Maurya, "Nonlinear adaptive volterra filter for control of distribution static compensator," *IEEE J. Emerg. Sel. Topics Power Electron.*, vol. 5, no. 1, pp. 559–567, Mar. 2017, doi: 10.1109/JESTPE.2016.2633481.

[23] A. Panda Kumar and M. Mangaraj, "DSTATCOM employing hybrid neural network control technique for power quality improvement," *IET Power Electron*, vol. 10, no. 4, pp. 480–489, Mar. 2017, doi: 10.1049/iet-pel.2016.0556.

[24] A. Sadiq, M. Usman, S. Khan, I. Naseem, M. Moinuddin, and U. M. Al-Saggaf, "q-LMF: Quantum calculus-based least mean fourth algorithm," in *Proc. 4th Int. Congr. Inf. Commun. Technol.*, 2020, pp. 303–311.

[25] U. M. Al-Saggaf, M. Moinuddin, and A. Zerguine, "An efficient least mean squares algorithm based on q-gradient," in *Proc. 48th Asilomar Conf. Signals, Syst. Comput.*, Nov. 2014, pp. 891–894, doi: 10.1109/ACSSC.2014.7094580.

[26] T. Ernst, *A Comprehensive Treatment of Q-Calculus*. Basel, Switzerland: Springer, 2012.

[27] J. Koekoek and R. Koekoek, "A note on the q-derivative operator," *J. Math. Anal. Appl.*, vol. 176, no. 2, pp. 627–634, Jul. 1993, doi: 10.1006/jmaa.1993.1237.